Bioactive Materials 8 (2022) 165–176

Contents lists available at ScienceDirect

Bioactive Materials

journal homepage: www.sciencedirect.com/journal/bioactive-materials

Spatiotemporally dynamic therapy with shape-adaptive drug-gel for the improvement of tissue regeneration with ordered structure

Ya-nan Fu [a], Yongsan Li [a,d], Bo Deng [b], Yingjie Yu [c,**], Fang Liu [b], Lei Wang [a], Guang Chen [a], Lei Tao [d], Yen Wei [d], Xing Wang [a,*]

[a] Beijing Advanced Innovation Center for Soft Matter Science and Engineering, Beijing Laboratory of Biomedical Materials, Beijing University of Chemical Technology, Beijing, 100029, China
[b] Department of Oncology of Integrative Chinese and Western Medicine, China-Japan Friendship Hospital, Beijing, 100029, China
[c] Institute of Translational Medicine, Shenzhen Second People's Hospital, The First Affiliated Hospital of Shenzhen University, Health Science Center, Shenzhen, 518035, China
[d] The Key Laboratory of Bioorganic Phosphorus Chemistry & Chemical Biology (Ministry of Education), Department of Chemistry, Tsinghua University, Beijing, 100084, China

ARTICLE INFO

Keywords:
Spatiotemporally dynamic therapy
Drug-gel
Shape-adaptive
Tissue regeneration
Ordered structure

ABSTRACT

A spatiotemporally dynamic therapy (SDT) is proposed as a powerful therapeutic modality that provides spatially dynamic responses of drug-carriers for adapting to the wound microenvironment. Herein, dynamic chitosan-poly (ethylene glycol) (CP) Schiff-base linkages are employed to perform SDT by directly converting a liquid drug *Kangfuxin* (KFX) into a gel formation. The obtained KFX-CP drug-gel with shape-adaptive property is used to treat a representative oral mucositis (OM) model in a spatiotemporally dynamic manner. The KFX-CP drug-gel creates an instructive microenvironment to regulate signaling biomolecules and endogenous cells behavior, thereby promoting OM healing by the rule of dynamically adjusting shape to fit the irregular OM regions first, and then provides space for tissue regeneration, over KFX potion control and the general hydrogel group of CP hydrogel and KFX-F127. Most interestingly, the regenerated tissue has ordered structure like healthy tissue. Therefore, the SDT provides a new approach for the design of next generation of wound dressing and tissue engineering materials.

1. Introduction

Tissue repair and regeneration with perfect structure remains a great challenge in the field of tissue engineering and regenerative medicine [1–4]. There is a highly sought-after goal to regenerate new tissue with ordered structure like healthy tissues. Although numerous traditional healing agents have been applied in the form of liquid and semisolid formulations [5–7], they always suffers from a short retention time and low drug concentration, consequently compromising the clinically therapeutic effect due to the loss of time-to-treat advantage [8–10].

Hydrogels, which can structurally and functionally mimic native tissue microenvironment, are one of the most widely used types of wound dressings and tissue engineering scaffolds [11–15]. As a promising intelligent drug delivery system and wound dressing, these biocompatible hydrogels possess time-to-treat advantages, such as adhering to wound defects and controlling and prolonging drug release [16–20]. Additionally, they can also provide a moist environment in the wound area, simultaneously allow the gas exchange between the wound and the external environment, absorb the wound exudates, and protect biologically active molecules from being altered, hence helping promote wound healing [21–24]. To date, many kinds of hydrogel-based commercial wound dressings have been used for wound healing and tissue regeneration. They are commonly constructed by natural polymers, including chitosan (eg. KytoCel®), alginate (eg. NU-GEL™), hyaluronic acid (Hyalofill®), collagen proteins (eg. Regenecare® Wound Gel) [21, 25–27]. Furthermore, hydrogels based on the single synthetic polymers or combination of natural and synthetic polymers mainly related to Pluronic® F127 hydrogel, polyacrylamide/poly-saccharide based

Peer review under responsibility of KeAi Communications Co., Ltd.
* Corresponding author.
** Corresponding author.
E-mail addresses: yuyingjie312@163.com (Y. Yu), wangxing@mail.buct.edu.cn (X. Wang).

https://doi.org/10.1016/j.bioactmat.2021.06.015
Received 28 January 2021; Received in revised form 8 June 2021; Accepted 11 June 2021
Available online 23 June 2021

FlexiGel®, agar/polyethylene glycol/polyvinylpyrrolidone based Neoheal® Hydrogel wound dressings [21,22,28]. However, unsatisfactory fittingness between the irregular damaged tissues and hydrogels could be easily observed at the interface due to the intrinsically poor shaping adaptivity [29]. Thus, most hydrogels lacks spatial advantages and are unable to dynamically adapt wound defects and further instruct endogenous cells to assemble into complete tissues structure [30].

To address these challenges, a dynamic shape-adaptive hydrogel is suitable for drug delivery to achieve the aforementioned unmet needs. Based on the dynamic Schiff base (imine, –N═CH–), biocompatible glycol chitosan (GC) and dibenzaldehyde-terminated poly(ethylene glycol) (DF-PEG) are good candidates to prepare a self-adapting CP hydrogel with shape-adaptive property. But, not all drug molecules could be loaded into the CP hydrogel network, some molecules even collapsed the Schiff base [31]. In addition, the direct conversion of clinically applicable potion into gel formulations (drug-gel), which do not lose the dose effect, is rarely reported so far. Therefore, we try to construct a dynamic shape-adaptive drug-gel to improve the therapy.

Kangfuxin (KFX) potion, a pure biologic medicine extracted from *Periplaneta americana*, mainly contains multiple amino acids, polyols, and small molecular peptides, *etc* [32,33]. The KFX potion can promote the cell increment, granulation tissue growth, angiogenesis, and ulcer healing, which has been widely used in the clinic as the ulcer or mucositis treatment [33]. However, the efficacy of KFX has been severely compromised due to poor delivery efficiency. Herein, we successfully converted liquid KFX into a dynamic gel formulation with Schiff base CP linkages, which is referred to as KFX-CP drug-gel (Scheme 1A and B). *This KFX-CP drug-gel neither compromises the efficacy of KFX potion nor disrupts gel structural integrity*. Due to the continuous cycle of breakage and regeneration of the inner crosslink network (Scheme 1C), this KFX-CP drug-gel is able to display dynamic shape-adaptive properties that could be translated to therapeutic advantages. Therefore, serious oral mucositis (OM), which frequently occurs in people who have undergone chemotherapy, was chosen as a model to verify the effect of healing and tissue regeneration. Clinical manifestation of OM is mainly ulceration. During this stage, oral mucosa and submucosal integrity is compromised and characterized large, deep ulcerations of the mucosa, which usually results in an irregular damaged surface of OM [34,35]. In our opinion, this KFX-CP drug-gel will prolong the retention time of KFX at the irregular OM region, and further create a dynamic biomimetic microenvironment to spontaneously provide adequate space for tissue upgrowth, achieving great therapeutic properties and improving tissue regeneration over traditional treatments (Scheme 1D). In view of the above-mentioned advantages of the KFX-CP drug-gel,

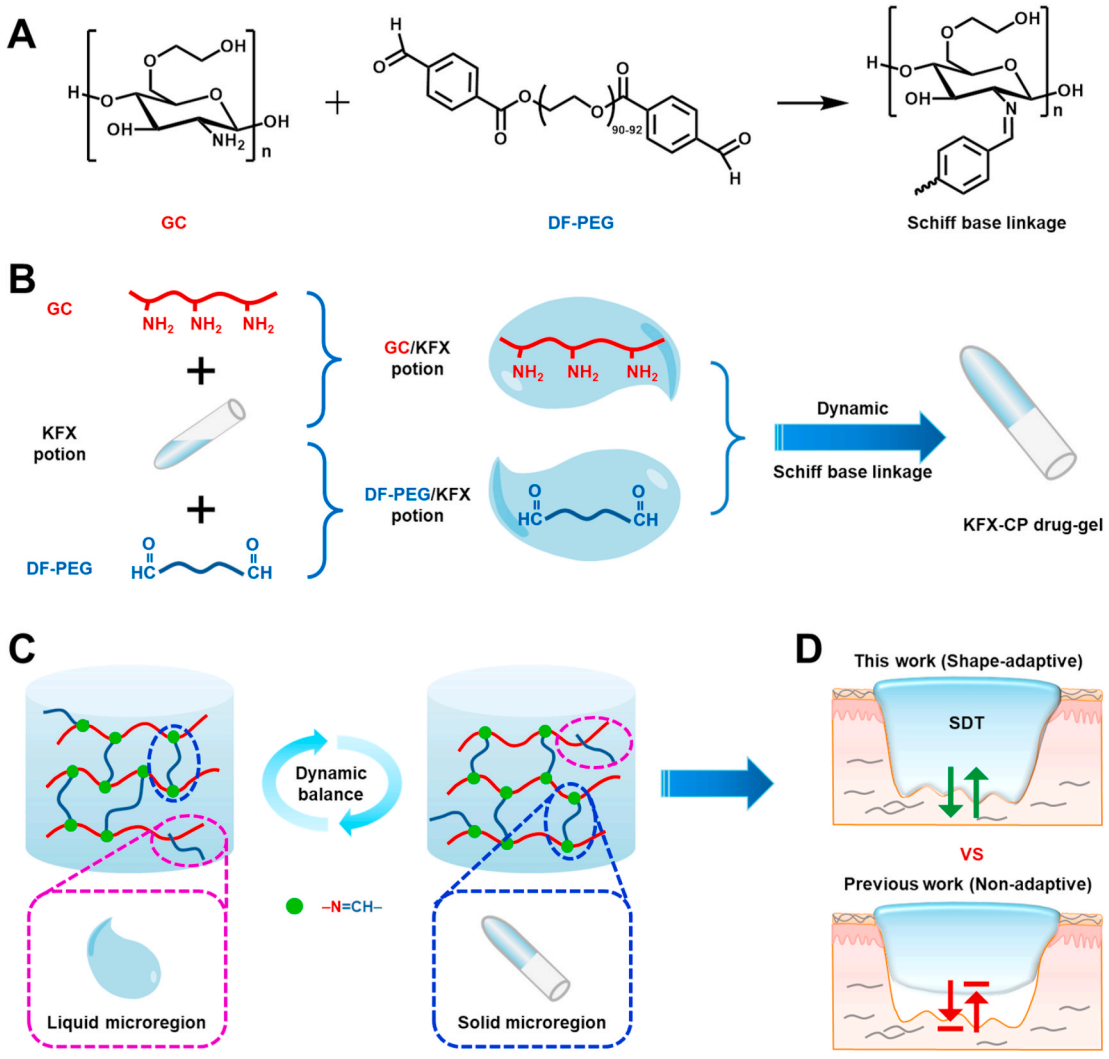

Scheme 1. Preparation of KFX-CP drug-gel and spatiotemporally dynamic therapy (SDT) for tissue regeneration. (A) The CP linkage preparation through the dynamic Schiff base between GC and DF-PEG. (B) Schematic representation of the KFX-CP drug-gel containing three components formed directly from the clinical KFX potion *via* CP Schiff base linkage. (C) Illustration of internal dynamic balance between liquid phase and solid phase microregions of KFX-CP drug-gel. (D) The SDT for improving tissue regeneration based on shape-adaptive KFX-CP drug-gel.

which provides spatially dynamic response of carrier for adapting to the wound microenvironment with long-lasting time curing of drug, we thus propose a new concept of spatiotemporally dynamic therapy (SDT).

2. Materials and methods

2.1. Materials

Poly (ethylene glycol) (PEG, Mw = 4000, 96%) was supplied by Sinopharm Group Co. Ltd. Glycol chitosan (GC, 82 kDa, 85% degree of deacetylation) was purchased from Wako Pure Chemical Industries, Ltd, Japan. *Kangfuxin* (KFX) potion was provided by China-Japan Friendship Hospital (Beijing, China). Pluronic® F127 powder (>98%) was purchased from Sigma Aldrich, USA. RPMI 1640 medium (RPMI 1640), penicillin-streptomycin (PS), fetal bovine serum (FBS), and trypsin were provided by Gibco Life Technologies (Beijing, China). The mouse fibroblast cells (L929) were obtained from Cell Resource Center, IBMS, CAMS/PUMC (Beijing, China). Rabbit anti-TNF-α antibody (1 mg mL^{-1}), rabbit anti-IL-6 antibody (1 mg mL^{-1}), goat anti-rabbit IgG/Alexa Fluor 594 antibody, goat anti-mouse IgG/Alexa Fluor 594 antibody and goat anti-rabbit IgG/FITC antibody were purchased from Beijing Boosen Biotechnology Co., Ltd (Beijing, China). RT products and PCR primers were provided by Beijing Dingguochangsheng Biotechnology Co., Ltd (Beijing, China). Anti-EGF antibody (rabbit), anti-VEGFA antibody [VG-1] (mouse) and anti-TGF-β1 antibody (rabbit) were obtained from Abcam Company, USA. All the other reagents (AR grade) were used as received from Sinopharm Chemical Reagent Co., Ltd (Shanghai, China) and used without further purification.

2.2. Preparation and characterization of DF-PEG

Dibenzaldehyde-terminated poly (ethylene glycol) (DF-PEG) was synthesized *via* esterification of hydroxyl terminated PEG with 4-formylbenzoic acid according to a previously reported method (Fig. S1) [36]. DF-PEG was obtained with a yield of 98% and was characterized by FT-IR (KBr, Fig. S2): ν (cm^{-1}) = 3492, 2884, 1978, 1719, 1468, 1347, 1282, 1106, 963, 844 and ^{1}H NMR (400 MHz, $(CD_3)_2SO$, δ, Fig. S3): 10.10 (s, 2H, C<u>H</u>O), 8.22 (d, J = 8.3 Hz, 4H, C<u>H</u>CCHO), 7.96 (d, J = 8.3 Hz, 4H, C<u>H</u>CHCCHO), 4.52–4.49 (m, 4H, COOC<u>H</u>$_2$), 3.86–3.83 (m, 4H, COOCH$_2$C<u>H</u>$_2$), 3.69–3.58 (m, 172–176H, OC<u>H</u>$_2$C<u>H</u>$_2$O).

2.3. Preparation of KFX-CP drug-gel

The KFX-CP drug-gel was prepared by directly converting KFX potion into a gel formulation *via* Schiff-base bonding reactions that took place at room temperature, as shown in Scheme 1. Briefly, the GC solution (3%, w/v) was prepared by dissolving GC (0.03 g) in KFX potion (1 mL), and the DF-PEG solution (10%, w/v) was obtained by dissolving DF-PEG (0.10 g) in KFX potion (1 mL). Afterwards, KFX-CP drug-gel was prepared by simply mixing the GC-KFX solution and the DF-PEG-KFX solution at a ratio of 3:1 (v/v) for approximately 1 min. The CP hydrogel was prepared following the procedure for the preparation of the KFX-CP drug-gel, where deionized water was used as solvent instead of KFX potion. As a control, KFX-F127 was also prepared. The KFX-containing Pluronic® F127 (KFX-F127), a widely used traditional thermal-sensitive hydrogel, was obtained by dissolving 0.14 g of Pluronic® F127 in a KFX potion (1 mL) directly. The sol-gel transformation of Pluronic® F127 was proved to occur when the temperature reaches 35 °C [37].

2.4. Characterization

^{1}H NMR was used to confirm the dynamic Schiff-base linkages in KFX-CP drug-gel. Scanning electron microscopy (SEM, JEOL JSM-7800 F, JEOL, Japan) was employed to observe the surface morphology of the freeze-dried KFX-CP drug-gel. The acceleration voltage of the SEM analysis is 10.0 kV. An AR-G2 rheometer (TA Instruments, USA) was applied to study the rheological properties and self-healing performances of the drug-gel. Confocal laser scanning microscopy (CLSM, Leica SP5, Germany) equipped with an argon/neon laser and a 63 × water immersion objective was used to observe the cell culture and biocompatibility.

2.5. Rheological property of KFX-CP drug-gel

A rheometer equipped with a 20 mm parallel-plate configuration was used to characterize the mechanical properties of the KFX-CP drug-gel. First, the gelation process was monitored. Typically, a GC-KFX solution (3%, 600 μL) was spread onto parallel plates of the rheometer, which was followed by the addition of a DF-PEG-KFX solution (10%, 200 μL) that was dropped uniformly onto the surface of GC. Then, storage moduli G' and loss moduli G'' were measured as a function of time to determine the gelation time. In addition, the modulus-frequency test of KFX-CP drug-gel was carried out using a steel plate (diameter: 20 mm) and was performed with 1% strain and 6.3 rad s^{-1}. The CP hydrogel with the same solid content was used as a control.

2.6. Shape-adaptability of KFX-CP drug-gel

For assessing the injectable property of KFX-CP drug-gel, dynamic KFX-CP was prepared in a syringe by mixing the GC-KFX solution and the DF-PEG-KFX solution. Then, the drug-gel was extruded directly through 23-gauge needles into Eppendorf tubes. To evaluate the shape-adaptability, the KFX-CP drug-gel (3 mL) was placed on top of green glass beads (diameter: 4 mm) in a vial and placed at room temperature. Photos were taken at 0, 1, and 2 h. As a control group, KFX-F127 (3 mL) was performed with the same procedure to compare the shape-adaptability of KFX-F127 and KFX-CP drug-gel. Additionally, the shape-adaptability of the KFX-F127 and KFX-CP drug-gel was further verified *via* a rheometer. A strain amplitude sweep (γ = 0.1–1000%) test was performed to determine the linear viscoelastic region and critical strain through modulus determination. Critical strain was defined when the KFX gels' modulus remarkably decreased. Afterwards, the KFX gels' modulus change was monitored under different applications of strains (larger/smaller than the critical strain). In addition, to examine the potential effects of the KFX on the cross-linking network, the modulus change of CP hydrogel under different applications of strains was tested.

2.7. Tissue mucoadhesive ability

The tissue mucoadhesive ability of KFX-F127 and KFX-CP drug-gel was determined according to a standard test method for strength properties of tissue adhesives in tension (ASTM F2258-05). The mass-distance curves, using porcine intestine as the mucous tissue, were recorded by a tensiometer (DCAT 21). After cleaning and cutting to a suitable size and shape (1 mm × 1 mm), the intestine was fixed to the substrate at 37 °C. The hydrogel solution was dropped on the lower mucosal surface before gelation. Then, the lower motor moved upwards to ensure sufficient contact between both pieces of intestine and solution. After complete conversion to gel, the motor was driven downward to perform the detaching step. The stress-distance curve indicated the dissociation force of the mucoadhesive strength, which was calculated as kPa.

2.8. In vitro drug release property

The KFX-127 (1 mL) and KFX-CP drug-gel (1 mL) was immersed in 20 mL of phosphate buffer saline (PBS, pH 7.4) and kept in a shaker (37 °C, 180 rpm), respectively. At a predetermined time interval (from 0 to 48 h), 1 mL of the solution was removed and replaced with an equivalent volume of fresh PBS. The released KFX was quantified by its absorbance at 222 nm, as determined by a UV–vis spectrophotometer and a standard

curve. All the experiments were repeated three times.

2.9. In vitro cell culture and biocompatibility

L929 cells (~5 × 10^6 cells per mL) were embedded in F127 and CP hydrogels in confocal dishes and covered with RPMI 1640 culture media (1 mL) that was supplemented with 10% FBS and 1% PS, respectively. Afterwards, the cell-laden hydrogels were incubated at 37 °C and 5% CO_2. After encapsulating 24 and 72 h, the cell-laden hydrogels were washed with PBS. Then, the cells were stained with fluorescein diacetate (FDA) and propidium iodide (PI). The cell-laden hydrogels were excited at wavelengths of 488 nm and 543 nm with CLSM to evaluate the cell viability and cell behavior in the hydrogels, respectively. The cell viability was reported as the percentage of the FDA stained cells compared to that of the total cells. Subsequently, the hydrogels were degraded with 1 mL of 3 wt% acetic acid solution, and the cells were re-suspended in 1 mL culture media. The cell counting of each hydrogel was carried out 3 times.

Furthermore, L929 cells (~5 × 10^3 cells per well) were seeded in 96-well plates. After 24 h incubation, equal volume fresh medium containing serial dilutions of GC (0–16 mg mL^{-1}) and DF-PEG (0–16 mg mL^{-1}) were added to replace the solution in the plate (n = 6). After 24 h of incubation, the cells were subjected to an MTT assay and absorbance values were measured by the spectrophotometry of microplate reader at 570 nm. The biocompatible results were calculated as the relative percentage of cell viability compared with the untreated cells.

2.10. In vitro degradation

In vitro hydrogel degradation was quantified in PBS solution (pH 7.4) [24]. The KFX-F127 and KFX-CP drug-gel (1 mL of each KFX gel) were placed in 5 mL of PBS solution and kept in a shaker (37 °C, 180 rpm), respectively. The residual weight (%) of the KFX gels was calculated from the following equation:

Residual weight (%) = $W_t/W_0 \times 100\%$, where W_0 is the initial weight of the KFX gels and W_t is the weight of the KFX gels at each predetermined time-point.

2.11. Animals

Thirty-six male Sprague Dawley rats (8 weeks old) were purchased from Beijing Vital River Experimental Animal Technique Ltd. Co. (License NO. SCXK [Jing] 2016–0006). All rats were housed at the SPF Animal Department of Clinical Institute in China-Japan Friendship Hospital (occupancy permit: SYXK (Jing) 2016–0020). Animals were acclimatized for 3 days before being used in experiments. All experimental animal protocols were performed according to the Guidelines of Beijing (China) for the Ethical Use of Animals (2010) and were authorized by the ethics committee of China-Japan Friendship Hospital (Approve number: 180202). All efforts were made to minimize animal suffering.

2.12. OM induction protocol and therapy

The protocol for the induction of OM was modified on the basis of a previously published protocol [38,39]. Rats under pentobarbital anesthesia (50 mg kg^{-1}, intraperitoneal) were treated with a round piece of filter paper (radius of 3 mm) soaked in acetic acid on both sides of the oral mucosa (1 min). OM could be clearly observed in the treated oral mucosal region after 24 h (recorded as day 0). Then, the 30 OM rats were randomly divided into 5 groups (n = 6). The treatments were KFX potion, CP hydrogel, KFX-F127, and KFX-CP drug-gel. Rats with OM treated by KFX, CP hydrogel and KFX-F127 were employed as positive controls. Rats with oral mucosa injuries that received no treatment were used as negative controls (Model). Medication started on day 0, when 200 μL of KFX potion, CP hydrogel, KFX-F127 and KFX-CP drug-gel were applied to the OM on both sides of rats once per day. As a sham treatment, 6 rats in the blank group (blank) received only pentobarbital anesthesia without acetic acid treatment. The OM healing processes were monitored throughout the whole treatment period (9 days). Measurements of OM areas through macroscopic photographs, food intake and body weights were performed daily (n = 6).

2.13. Histology analysis

Inflammation and tissue regeneration in the OM area were evaluated by hematoxylin-eosin staining (H&E) [40]. All rats were sacrificed after 9 days of treatment, and oral mucosa tissues on each side were extracted from animals under deep anesthesia (pentobarbital, 100 mg kg^{-1}, intraperitoneal administration) [39]. Afterwards, oral mucosa tissues were immediately fixed by incubation in 4% paraformaldehyde for 24 h; then, they were dehydrated and embedded in paraffin. All paraffin blocks were sliced into sections (4 μm thick) for H&E staining, and stained slides observed under an optical microscope equipped with a CCD camera.

2.14. Immunohistochemistry analysis

After 9 days of treatment, the OM areas were immunohistochemically stained with the proinflammatory cytokines TNF-α and IL-6 by using standard protocols [41]. Briefly, the deparaffinized and hydrated tissue sections (4 μm thick) were incubated overnight with anti-TNF-α and anti-IL-6 antibodies. Afterwards, the sections were incubated for 15 min with a biotin-labeled secondary antibody and a horseradish peroxidase-labeled streptavidin. Finally, TNF-α and IL-6 were visualized using chromogen 3,3′-diaminobenzidine (DAB) for 2–10 min. Three views were randomly chosen per tissue section for photography with a digital imaging system. The integrated option density (IOD) of TNF-α or IL-6 staining per view was measured using Image-Pro Plus (IPP) software (Media Cybernetics, USA).

2.15. Real-time PCR analysis

mRNA expression of TNF-α and IL-6 in each group was detected by quantitative real-time polymerase chain reaction (q-PCR) [42]. Oral mucosal tissues were extracted on day 9 and immediately immersed in liquid nitrogen before being frozen at −80 °C [43]. After homogenization, total RNA of the oral mucosal tissues was extracted with Trizol reagent. Reverse transcription reactions for synthesizing first-strand cDNA were performed using reverse transcriptase and 30 μg of total RNA. The primer sequences are listed in Table S2. The threshold cycle (CT) was recorded to express the value of each sample. The DDCT method was used to quantify relative expression [44].

2.16. Immunohistofluorescent staining analysis

Immunofluorescence staining of tissue sections was performed to study OM healing. Epidermal growth factor (EGF), transforming growth factor-β1 (TGF-β1) and vascular endothelial growth factor (VEGF) are three main growth factors involved in the healing process of OM [45,46]. In short, paraffin-embedded oral mucosa tissues were first cut into 5 μm sections, and then the sections were stained by incubation overnight at 4 °C with anti-EGF antibody (rabbit), anti-VEGFA antibody [VG-1] (mouse) and anti-TGF-β1 (rabbit). A goat anti-rabbit IgG/Alexa Fluor 594 antibody, a goat anti-mouse IgG/Alexa Fluor 594 antibody and a goat anti-rabbit IgG/FITC antibody were used as the secondary antibodies to reveal EGF, VEGF and TGF-β1 expression. Finally, DAPI was employed to stain the cell nuclei.

2.17. Statistical analysis

Numerical data are expressed as means ± standard deviation.

Statistical analyses of all test data were analyzed using ANOVA with Tukey's post-hoc analysis (IBM SPSS, USA). A P value of less than 0.05 was considered significant.

3. Results and discussions

3.1. Preparation and characterization of KFX-CP drug-gel

This work aims to show the superiority of SDT for OM based on the new type of shape-adaptive KFX-CP drug-gel. DF-PEG was synthesized *via* esterification of hydroxyl terminated PEG with 4-formylbenzoic acid according to a reported method (Fig. S1) [36]. GC and DF-PEG were dissolved with KFX potion and then were mixed to quickly form CP cross-linkages and produce a drug-gel, demonstrating that liquid KFX could be used in gel formation through this method (Fig. 1A). The dynamic Schiff-base linkage in KFX-CP drug-gel was confirmed through a model experiment. Glucosamine (GSA), the basic unit of chitosan, was employed as a model molecule to react with DF-PEG. As shown in the ^{1}H NMR spectrum (Fig. S4), the significant peak of Schiff-base could be noticed. As revealed by the SEM image in Fig. 1B and Fig. S5, the KFX-CP drug-gel exhibited a 3D structure with wrinkles, which may be caused by KFX-induced gel swelling and GC itself [47,48]. Furthermore, this kind of wrinkle morphology may provide enough surface roughness to fit uneven surface area in oral mucosa region. Rheology analysis was then carried out to evaluate the mechanical properties of the KFX-CP drug--gel. As shown in Fig. 1C, after the addition of the DF-PEG-KFX solution (10% w/v, 200 μL) to the GC-KFX solution (3% w/v, 600 μL), the storage modulus (G') gradually increased, and it surpassed the loss modulus (G'') after approximately 60 s, indicating the rapid formation of a crosslinked gel network.

A frequency sweep (1–100 Hz, Fig. S6B) showed that the elastic moduli G' of the KFX-CP drug-gel (~4500 Pa) was consistently greater than the G'', indicating a stable and typical solid-like rheological behavior. Moreover, the KFX-CP drug-gel exhibited larger elastic moduli than that of CP hydrogel (~3900 Pa, Fig. S7A), demonstrating the KFX components can increase the mechanical strength of CP hydrogel and show no damage to the cross-linked network. Afterwards, a strain amplitude sweep (γ = 0.1–1000%, Fig. S6C) test explored the elastic response of the KFX-CP drug-gel. The G' value decreased rapidly above the critical strain region (γ = 25%, from ~4300 Pa to 13 Pa), suggesting the collapse of the KFX-CP drug-gel network.

Due to the intrinsic dynamic equilibrium of the Schiff-base bond, the KFX-CP drug-gel is able to rebuild its hydrogel network through the continuous regeneration and cleavage of the imine bond [49]. This imine bond endows the system with excellent self-adaptability. Its strain-induced damage and self-healable properties were then investigated with a rheometer. The KFX-F127 and KFX-CP drug-gel were tested through a continuous step change of oscillatory strain between 200% and 1% under a constant frequency (1 Hz, Fig. 1D and Fig. S8). In brief, the G' value of the KFX-CP drug-gel decreased sharply from ~4300 Pa to 82 Pa at a large dynamic strain (γ = 200%, Fig. 1D), which suggests that the breakdown of the hydrogel network is due to the dissociation of the Schiff-base linkages. Then, the G' value instantaneously recovered to its initial value (~4300 Pa) after application of a low strain (γ = 1%, Fig. 1D). This indicated the recovery of the inner structure of the KFX-CP drug-gel, which was similar to that of the original CP hydrogel (Fig. S7B), showing the KFX components have no effect on the self-healing and self-adaptability of CP hydrogel. However, with a low strain value (γ = 1%), the G' of KFX-F127 could not restore to its original values (Fig. S8), revealing the unrecovery of the inner microstructure after a higher strain-induced structural damage. Hence, the transition shown above substantiated the self-healing property of the KFX-CP drug-gel, which indicates that the KFX-CP drug-gel has more sufficient shape-adaptability.

Based on the recovery property, the KFX-CP drug-gel was determined to be injectable. After loading in a syringe and injecting with a 23-gauge needle, KFX-CP drug-gel formation regenerated after 4 h (Fig. 1E). In addition, the KFX-CP drug-gel was placed above two layers of green beads. It flowed down gradually in the manner of a viscous fluid through the narrow gap of the green beads and finally engulfed the green beads at the bottom of the vial after 2 h (Fig. 1F). Conversely, the control KFX-F127 slightly moved down without encapsulating green beads at the bottom within 2 h (Fig. S9). These experiments proved that the inner dynamic network could lead to the outstanding mobility and shape-adaptability of the KFX-CP drug-gel.

To achieve the desired therapeutic efficacy, hydrogels used for tissue are required to firmly adhere to the moist tissue surface and resist mechanical forces in a dynamic environment [50]. Therefore, the tissue mucoadhesive ability of the KFX-CP drug-gel was evaluated according to a standard protocol (ASTM F2258-05) using a tensiometer (DCAT 21, porcine intestine model, Fig. 1G and H). The mucoadhesive strength of KFX-CP drug-gel on a porcine intestine was nearly 1.20 kPa (Fig. 1H), which was 2-fold higher than that of KFX-F127 (0.58 kPa); these results satisfied the requirement of adhering to tissues [51]. Owing

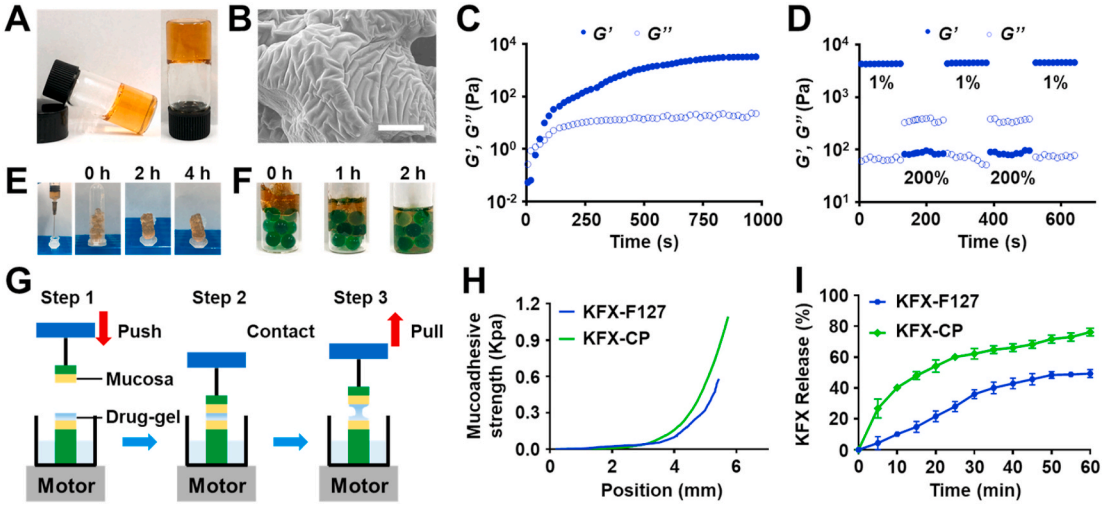

Fig. 1. Characterization of the KFX-CP drug-gel. (A) Photograph of the drug-gel. (B) SEM image of the drug-gel; the scale bar is 10 μm. (C) Rheological properties of the gelation process and (D) the damage-self-healing property *via* continuous stepwise increasing strain (from 1% to 200% alternately) at 25 °C. (E) Injectability test with a 23-gauge needle. (F) Shape-adaptive test with stacking beads. (G) Test system and (H) mucoadhesive strength of KFX gels on a porcine intestine. (I) Cumulative release profile of KFX from KFX-F127 and KFX-CP drug-gel in PBS (pH 7.4) within the first 1 h (n = 3).

to the strong adhesion to the tissue surface, the KFX-CP drug-gel was suitable for OM administration. It not only filled wound defects with irregular shapes [52] but also prolonged the retention time of KFX and achieved effective drug release in situ, thereby accelerating the process of OM healing. The KFX-CP drug-gel, with a drug encapsulation efficiency of 100%, was then submerged in PBS for an accumulative drug release study (Fig. 1I, see Fig. S10A for the test model). KFX was quickly released (~76.2%) from the drug-gel within the first 1 h, which was significantly higher than that of KFX-F127 (~49.4%). After that, a relatively steady and sustained release of KFX (~99.2%) lasted until the gel was completely degraded at 48 h, however, the KFX cumulative release from KFX-F127 was ~82.3% (Fig. S10B). These results indicated KFX-CP drug-gel had a better drug release ability, making it become a much promising delivery system for delivering KFX for efficient OM healing.

Hydrogels based wound-dressings should be biodegradable in wound healing and tissue regeneration [23,24]. The degradation rate of two KFX gels was shown in Fig. S11. The KFX-CP drug-gel degraded faster in the first 1 h (~60.8%), followed by gradually full degradation within 48 h. However, the weight of KFX-F127 decreased much slower with incomplete degradation than that of KFX-CP drug-gel (only ~54.3% at 48 h). These results suggest that the KFX-CP drug-gel is more suitable for *in vivo* OM treatment and oral tissue regeneration during each therapy based on its excellent performance in degradation.

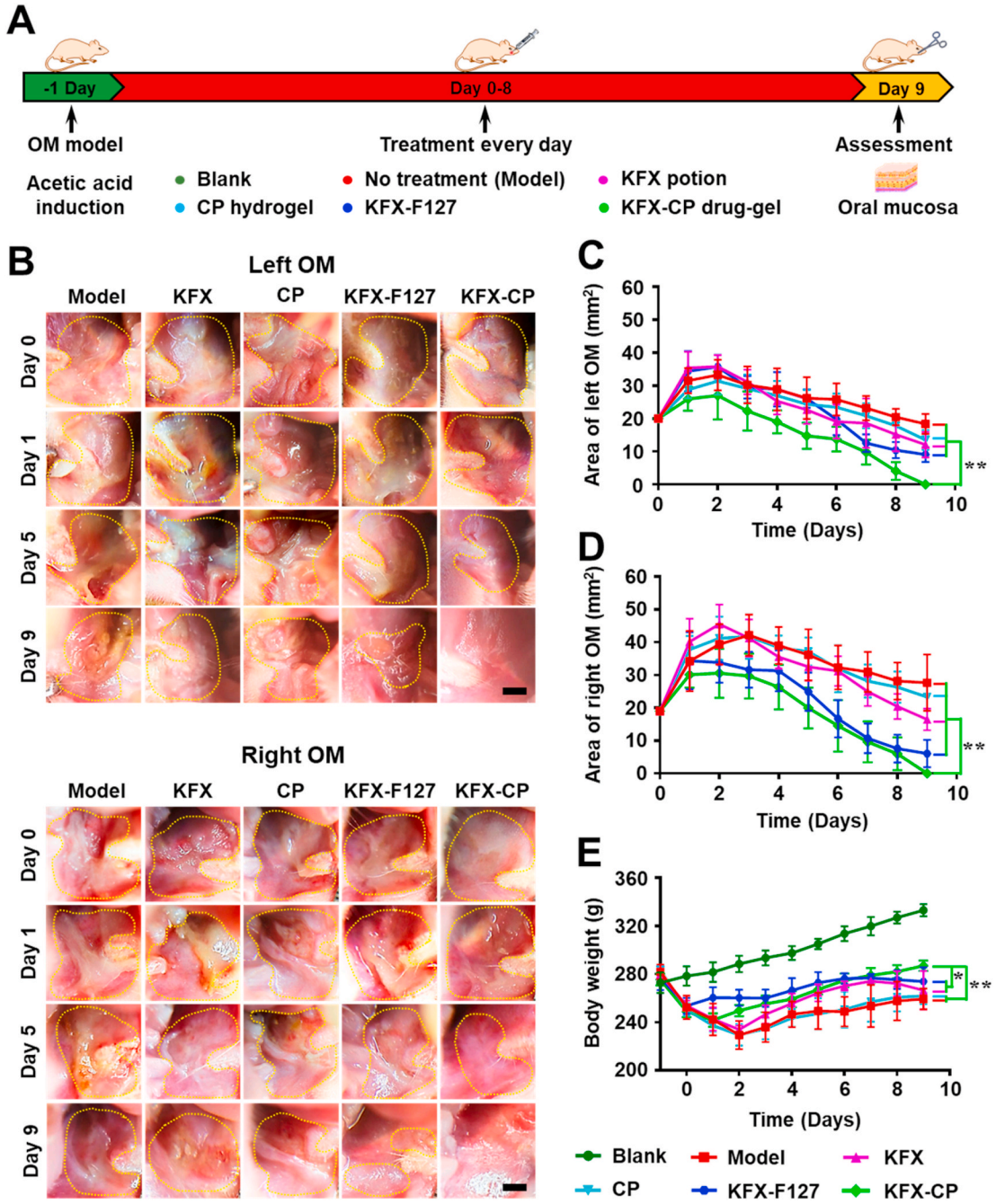

Fig. 2. *In vivo* OM healing study. (A) Schematic diagram of the experimental process. (B) Representative images of left and right side OM within 9 days of administration. The scale bar is 1 mm. The corresponding statistical diagram of the (C) left and (D) right OM area of rats in (B). (E) Body weight changes during treatment. The results are expressed as the mean ± SD in all groups (n = 6). *P < 0.05, **P < 0.01, compared with KFX-CP drug-gel at day 9.

3.2. In vivo OM healing

Encouraged by the attractive shape-adaptability and favorable tissue adhesiveness of the KFX-CP drug-gel, we attempted to utilize it for OM treatment. Fig. 2A shows the protocol for induction and therapy of the OM model in rats. OM healing conditions are shown in Fig. 2B for the different groups: the control model (no treatment), KFX, CP hydrogel, KFX-F127 and KFX-CP drug-gel groups. The OM treated with KFX-CP drug-gel exhibited faster healing efficiency than the other positive controls (KFX, CP hydrogel and KFX-F127). Upon visual inspection, the posttreatment oral mucosa following KFX-CP drug-gel application appeared to have a smooth surface and healthy color after 9 days of treatment. In contrast, OM was still clearly observed in other groups. Moreover, the therapeutic effect was also analyzed according to the OM area (Fig. 2C and D). Similar results revealed that the KFX-CP drug-gel group had the best OM healing area (area of OM: 0 mm^2) among all test groups after 9 days of treatment. These results preliminarily indicated complete healing of the OM. OM is usually associated with decreased food intake and body weight [53,54]. Hence, the condition of all rats after operation was carefully monitored. As shown in Fig. 2E, due to the low food intake (Fig. S12), the body weight of rats with OM decreased significantly beginning on day 0, which was followed by a steady increase with each subsequent administration. After 9 treatments, the body weight within the KFX-CP drug-gel group was higher than that of all other groups. This result is most likely due to the suitable tissue adhesiveness of KFX-CP drug-gel, which could protect the oral mucosa from external stimulation more effectively than other treatments.

3.3. Histological evaluation of OM healing and ordered regenerative structure

Since re-epithelialization is an important process in wound healing [55], hematoxylin eosin (H&E) staining was performed on OM sections to further understand the healing process. Fig. 3A and Fig. S13 clearly showed that the epithelial structure completely disappeared in the model group (no treatment) compared with that of the blank group. The ulcer reached deep into the spinous layer, and the cells above the spinous layer were irregular. No clear edges could be observed in the spinous layer. The epithelial cells were degenerated, necrotic and fell off, leaving the exposed lamina propria of tissues due to the destruction of the mucosal surface. Moreover, karyopyknosis and vacuolization of the cytoplasm were observed. In the positive control groups (KFX, CP hydrogel and KFX-F127), the pathologic changes of OM regions remained distinctly visible, although they healed much better than they did in the model group (no treatment) after 9 days of treatment. It is worth noting that the KFX-CP drug-gel treated sections showed nearly complete epithelialization and normal connective tissue. Epidermal cells and epithelial layer fibroblasts tended to arrange regularly and closely. In addition, the injured oral mucosa tissue was completely covered by healthy epithelial tissue, and no visible fibrosis was observed after 9 days of treatment. The cells of the basal layer, spinous layer, granular layer and keratinized layer were arranged in an orderly manner. The cytoplasm and nucleus were clear and had no

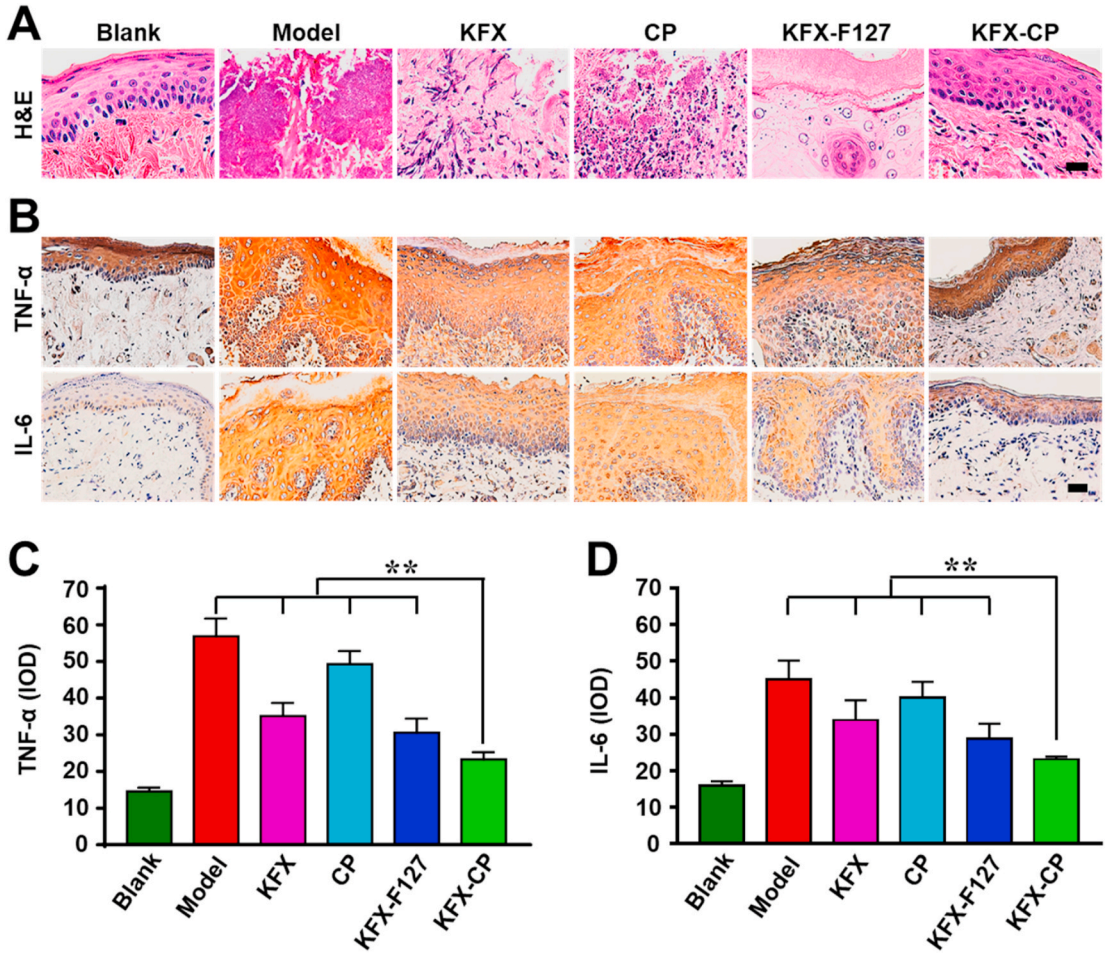

Fig. 3. Evaluation of tissue regeneration after OM. (A) Histomorphological evaluation of all test groups after 9 days. The scale bar is 20 μm. (B) Photograph analysis of immunohistochemical staining in each group. Comparison of immunohistochemical expression of TNF-α (C) and IL-6 (D) in oral mucosal tissues. The scale bar is 40 μm. The results are expressed as the mean ± SD in all groups (n = 6). **P < 0.01, compared with KFX-CP drug-gel.

abnormality and vacuolization; further, the structure of the epidermis was clear, having no scar formation in fibrous connective tissues. It is clear that the regenerated oral mucosal tissue was almost as thick as that of the healthy control, possessing an ordered structure similar to that of normal tissue, highlighting that the KFX-CP drug-gel was beneficial to OM tissue remodeling and regeneration, inducing well-organized arrangement.

To more directly assess the inflammation and healing of OM, immunohisto-chemistry experiments were employed. OM tissues were labeled with two typical proinflammatory factors, tumor necrosis factor-α (TNF-α) and interleukin-6 (IL-6), to evaluate the inflammatory condition [45,56,57]. In Fig. 3B, a large number of inflammatory cells stained with TNF-α or IL-6 (yellow) appeared in un-treated, KFX-, CP- and KFX-F127-treated OM tissues, suggesting a severe inflammatory response. Although the accumulation and activation of inflammatory cells is essential for initiating inflammation into the repair stage, excessive inflammation may lead to tissue damage and a delay in OM healing [58–60]. In contrast, little secretion of TNF-α and IL-6 cytokines was observed in the KFX-CP drug-gel group, which is most likely due to that group maintaining a more appropriate inflammatory environment that was conducive to OM healing than the other groups. Furthermore, the quantitative IOD results (Fig. 3C and D and Table S1) indicated that the KFX, CP hydrogel and KFX-F127 treatments resulted relatively lower levels of both TNF-α (IOD: 35.12 for KFX; 49.31 for CP; 30.58 for KFX-F127) and IL-6 (IOD: 33.86 for KFX; 39.97 for CP; 28.76 for KFX-F127) gene expression compared to that of the model group (no treatment, TNF-α: 56.83; IL-6: 45.06), but it was still much higher than that of the blank group. The KFX-CP drug-gel group exhibited the lowest expression of TNF-α (IOD: 23.26) and IL-6 (IOD: 23.11) compared to that of the KFX, CP and KFX-F127 groups, indicating a much effective recovery from the inflammatory response. These results demonstrated that the potential anti-fibrotic benefit of KFX-CP drug-gel, which could transition fibroblast toward a more normal, healthy phenotype and promote OM healing [57].

To confirm the expression of inflammatory factors at the gene level, q-PCR was conducted to determine the mRNA expression on day 9 of the treatments. The q-PCR data (Fig. S14) revealed that although TNF-α and IL-6 mRNA levels of KFX, CP hydrogel and KFX-F127 groups were significantly downregulated compared with those of the negative group (Model), none of them was as effective as the KFX-CP drug-gel. Importantly, the expression of TNF-α (6.46%) and IL-6 (7.23%) mRNA in the KFX-CP drug-gel group was nearly the same as that of blank control animals (TNF-α: 1.81%; IL-6: 1.84%, Table S3), which revealed significantly suppressed inflammation on OM.

Additionally, immunofluorescence staining was used to further explore the molecular mechanism behind OM healing and oral mucosa regeneration. The expression of three main growth factors, EGF, TGF-β1 and VEGF, was determined in OM areas. These growth factors are signaling molecules that regulate events in tissue development and repair, including cell proliferation, differentiation, and migration [61,62]. After 9 days of treatment, the KFX-CP drug-gel group held stronger fluorescence signals for EGF (red), VEGF (red) and TGF-β1 (green) than the other groups (Fig. 4A and B). These growth factors are extensively distributed in oral mucosal tissues, which are essential for OM repair and mucosal tissue regeneration. These growth factors also displayed substantially more deposition in the KFX-CP drug-gel group (EGF:

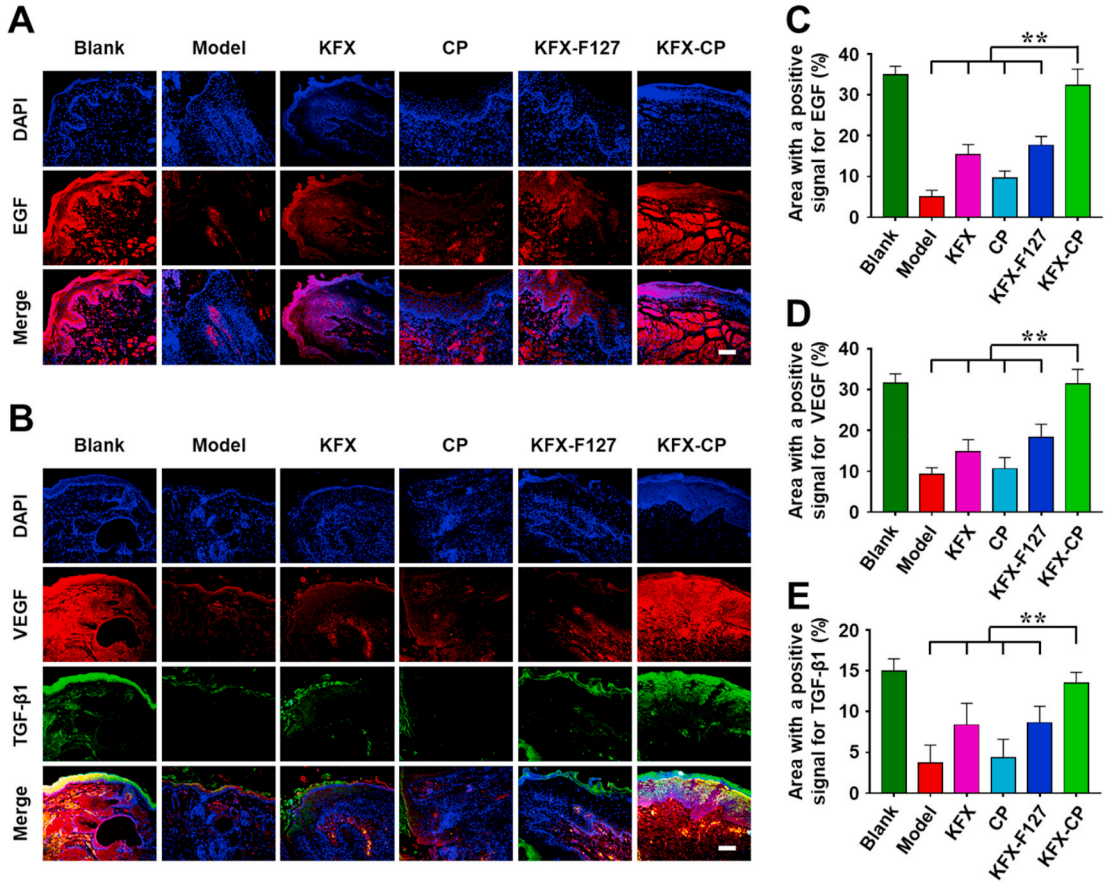

Fig. 4. Qualitative and quantitative analyses of growth factors associated with OM healing. (A) EGF (red) and (B) VEGF (red) and TGF-β1 (green). The cell nuclei were stained blue. The scale bar is 50 μm. Quantified data of the area percentage covered by (C) EGF, (D) VEGF and (E) TGF-β1. The results are expressed as the mean ± SD in all groups (n = 6). **P < 0.01, compared with KFX-CP drug-gel. (For interpretation of the references to color in this figure legend, the reader is referred to the Web version of this article.)

32.39%, VEGF: 31.32%, and TGF-β1: 13.51%) than in the other groups (Fig. 4C–E, $P < 0.01$), and their levels were nearly equivalent to those of the blank groups (EGF: 34.95%, VEGF: 31.62%, and TGF-β1: 14.96%). The higher expression of growth factors was essential for OM healing and tissue regeneration. During the repair process, EGF can accelerate keratinocyte migration and substantially increase fibroblast proliferation, thus promoting re-epithelialization and recovery of oral mucosal tissue integrity [46,63]. In addition to EGF, both VEGF and TGF-β1 play an important role in well-organized oral mucosa tissue remodeling during the OM healing process. VEGF is essential in angiogenesis, re-epithelialization and collagen deposition [64]. Meanwhile, TGF-β1 can facilitate the formation of granulation tissue by increasing the expression of genes associated with extracellular matrix (ECM) formation, including fibronectin, the fibronectin receptor, and collagen and protease inhibitors [65]. It is also involved in upregulating the angiogenic growth factor VEGF [66]. All of these positive findings suggested that the shape-adaptive KFX-CP drug-gel could effectively promote OM healing and help return injured mucosa tissues to health.

3.4. Biological mechanism of tissue regeneration with ordered structure

The significant acceleration of *in vivo* OM healing, oral mucosa tissue regeneration and maintenance of an ordered structure was shown in the KFX-CP drug-gel group (Figs. 3 and 4). This is likely related to the spatiotemporally dynamic property of the KFX-CP drug-gel, which achieved effective KFX retention and superior dynamic shape-adaptability in OM areas (Fig. 5, KFX-CP drug-gel). The KFX-CP drug-gel displayed dynamic hydrogel properties due to the Schiff-base bond. It increased the degree of matching and mucoadhesion between the drug-gel and wound surface and significantly prolonged the amount of time KFX spent at the site of the OM defects, avoiding the loss observed with liquid KFX (Fig. 5, KFX potion) [54,67]. Therefore, the KFX-CP drug-gel possessed time-to-treat advantages and promoted OM healing over a longer timescale. Simultaneously, by dynamic adjusting its shape, the KFX-CP drug-gel was able to seamlessly adhere to the irregular surfaces of OM and to provide abundantly moist conditions [16], thereby spatially establishing a suitable niche for achieving accelerated OM repair. The concerted action of these superior temporal and spatial characteristics allow the KFX-CP drug-gel to actively interact with OM defects, during which it clearly inhibited the inflammatory response (Fig. 5, also see Fig. 3 for details) and significantly upregulated the expression of growth factors (Fig. 5, also see Fig. 4 for details), and further instructed endogenous cells to proliferate, migrate and reconstruct. Meanwhile, the KFX-CP drug-gel spontaneously provides space for new tissue upgrowth based on its dynamic shape-adaption (Fig. 5, KFX-CP drug-gel) and rapid degradation (Fig. S11). In addition, the KFX-CP drug-gel could also mimic native ECM for different signaling molecules to communicate and coordinate to restore the complete tissue structure [4,68,69]. These spatiotemporal treatment advantages gave rise to extraordinary OM healing and oral mucosa tissue regeneration with ordered structure by activating different signaling pathways and regulating endogenous cells behavior.

Conversely, although KFX-F127 can also control KFX release, it was unable to spontaneously fit with the defective surface of OM, leading to unknown or neglected spatial barriers (Fig. 5, KFX-F127). Moreover, it could not provide enough space during the process of endogenous tissue regeneration due to poor shape-adaptability and slow degradation (Fig. S11). Of course, the disadvantage of liquid KFX for in-site cure was the insufficient time of treatment (Fig. 5, KFX potion). These defects in both the KFX potion and KFX-F127 result in the wound not being

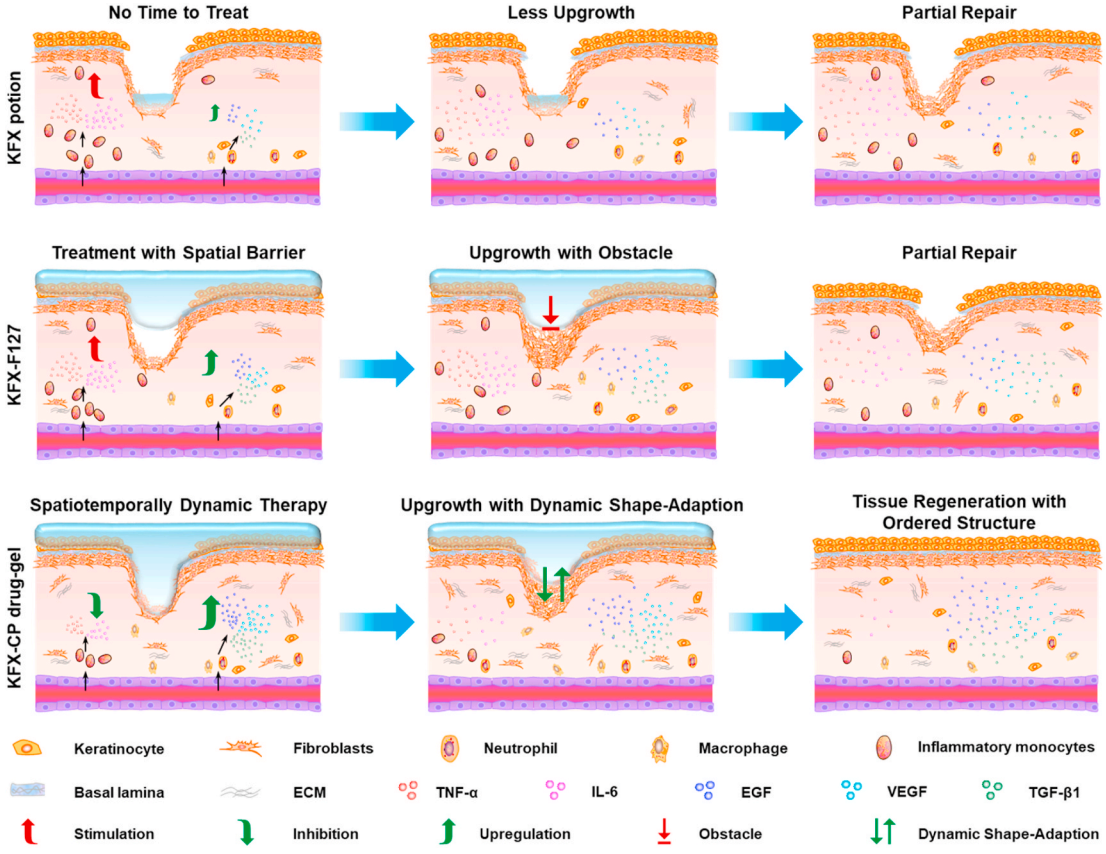

Fig. 5. Biological mechanism of SDT in the OM healing model. OM healing and mucosa tissue regeneration under treatments of KFX potion, KFX-F127, and KFX-CP drug-gel, at which only SDT based on KFX-CP drug-gel could enable tissue regeneration that recovered ordered structure, which is consistent with the pathological results in Fig. 3A.

covered completely, causing excessive stimulation of the secretion of inflammatory factors. Generally, in the early stage of wound healing, the accumulation and activation of inflammatory cells are crucial for the transition from inflammation to the repair phase. However, excessive inflammation delays the process of wound healing [59,70]. Therefore, the overexpression of proinflammatory factors (TNF-α and IL-6) in the KFX potion and KFX-F127 treatments prolonged the inflammatory phase, resulting in delayed OM healing (Fig. 5, also see Fig. 2 for details) and blocked tissue regeneration (see Fig. 3 for details).

The spatiotemporal advantages of the KFX-CP drug-gel can be further explained by the biocompatibility between the F127 hydrogel and the self-adapting CP hydrogel. L929 cells were cultured in F127 and CP hydrogels (Fig. S15A). After 24 and 72 h of incubation, most of the cells survived in the CP hydrogel (green dots). Meanwhile, the cell viability (Fig. S15B) was as high as 99.9% and 97.2% for CP hydrogel after 24 and 72 h culture, respectively. The total cell numbers after 72 h cultivation showed distinct increasing compared with that the original hydrogel (Fig. S15C), which indicated that the L929 fibroblast cells could grow well and proliferate significantly in the CP hydrogel. Furthermore, cytotoxicity of GC and DF-PEG in hydrogel was also evaluated. L929 cells lived well (~86.4%) after culture with GC or DF-PEG (16 mg mL^{-1}) for 24 h (Fig. S15D), demonstrating the excellent biocompatibility of the CP hydrogel. However, F127 was not suitable for cell culture due to its short gel incubation, poor tissue adhesion and mechanical properties, and cellular toxicity at high concentrations [71–73]. Almost all dead cells (red dots) were observed in the dyed confocal after a 24 h culture (cell viability: 1.8%, Figs. S15A–C), which is consistent with previous reports [71,74]. These results not only suggested that the CP hydrogel created a cell friendly environment but also provided proof of the superior 3D spatiotemporal microenvironments for tissue regeneration. In other words, by mimicking the spatiotemporal alterations in the native ECM, the KFX-CP drug-gel can largely affect cell behaviors, including cell proliferation, migration, and self-renewal, in both spatial and time dimensions [69]. Therefore, the 3D SDT cell niches constructed by the KFX-CP drug-gel played a crucial role in promoting OM healing and enabling ulcer lesions to recover and regain normal physiological structure. Overall, due to the dynamic, synergistic temporal and spatial regulation of cell viability, signaling biomolecules and endogenous cell behaviors, the KFX-CP drug-gel promoted significant OM healing and further restoration of the damaged tissues to their original ordered structures.

4. Conclusions

In summary, SDT was realized on the model of OM *in vivo*. The direct conversion of KFX potion into a gel formulation was successfully achieved to verify SDT. The dynamic shape-adaptive responses based on the Schiff-based CP networks of the drug-gel played a crucial role in SDT. In addition, relative to other methods, this smart drug-gel exhibited many desirable features, such as improved tissue adhesiveness, a higher drug release rate and good biocompatibility. These advantages are thought to enable the KFX-CP drug-gel with the ability to provide a spatially and temporally dynamic therapeutic option, which is suitable for treating irregular tissue wounds. Based on the SDT ability, the KFX-CP drug-gel spontaneously fitted the uneven OM area by adjusting its shape and achieved effective retention of KFX potion, and then efficiently regulated different signaling biomolecules and instructed endogenous cells behavior. In particular, by spontaneously providing enough space for new tissue growth, this spatiotemporally dynamic drug-gel promoted tissue regeneration with ordered structure that was similar to that of healthy oral mucosa. These results further highlighted the internal connection between SDT and tissue regeneration to produce an ordered structure. Taken together, these data show that the spatiotemporally dynamic drug-gel is a superior wound dressing option for irregular wound healing, tissue regeneration with ordered structure and no scar formation. Therefore, SDT provides a promising approach for designing and generating smart scaffolds for wide biomedical applications.

Declaration of competing interest

The authors declare that they have no known competing financial interests or personal relationships that could have appeared to influence the work reported in this paper.

CRediT authorship contribution statement

Ya-nan Fu: Design of experiments, Materials preparation and evaluation, Animal experiment, Data curation, Writing – original draft, Writing-Original draft preparation. **Yongsan Li:** Chemical and biocompatible experiments, Data curation. **Bo Deng:** Providing the protocol for creating of OM model, Histological evaluation and data analysis, Funding acquisition. **Yingjie Yu:** Writing-review and editing, Supervision, Funding acquisition. **Fang Liu:** Immunohistofluorescent staining experiment and data analysis, Funding acquisition. **Lei Wang:** PCR experiment and data analysis. **Guang Chen:** PCR experiment and data analysis. **Lei Tao:** Assisted in evaluating of materials, Writing – review & editing. **Yen Wei:** Assisted in evaluating of materials, Writing – review & editing. **Xing Wang:** Design and interpretation of study, Writing – review & editing, Supervision, Project administration, Funding acquisition.

Acknowledgments

This work was supported by Key Program of Beijing Natural Science Foundation (Z200025), National Natural Science Foundation of China (52003161), National Mega-project for Innovative Drugs (2019ZX09721001-007-002), Shenzhen Science and Technology Project (JCYJ20180507183842516), Fundamental Research Funds for the Central Universities (BHYC1705B, PYBZ1709) and Research Projects on Biomedical Transformation of China-Japan Friendship Hospital (PYBZ1806).

Appendix A. Supplementary data

Supplementary data to this article can be found online at https://doi.org/10.1016/j.bioactmat.2021.06.015.

Declaration of competing interest

The authors declare that they have no known competing financial interests or personal relationships that could have appeared to influence the work reported in this paper.

References

[1] G.C. Gurtner, S. Werner, Y. Barrandon, M.T. Longaker, Wound repair and regeneration, Nature 453 (2008) 314–321.
[2] T.S. Stappenbeck, H. Miyoshi, The role of stromal stem cells in tissue regeneration and wound repair, Science 324 (2009) 1666–1669.
[3] M.C.Y. Heng, Wound healing in adult skin: aiming for perfect regeneration, Int. J. Dermatol. 50 (2011) 1058–1066.
[4] G.M. Sun, Y.-I. Shen, J.W. Harmon, Engineering pro-regenerative hydrogels for scarless wound healing, Adv. Healthcare Mater. 7 (2018) 1800016.
[5] R.F. Pereira, P.J. Bartolo, Traditional therapies for skin wound healing, Adv. Wound Care 5 (2016) 208–229.
[6] R.L. Thangapazham, S. Sharad, R.K. Maheshwari, Phytochemicals in wound healing, Adv. Wound Care 5 (2016) 230–241.
[7] Y.K. Luo, M. Feng, Z.X. Fan, X.D. Zhu, F. Jin, R.Q. Li, J.B. Wu, X. Yang, Q.H. Jiang, H.F. Bai, Y.C. Huang, J.Y. Lang, Effect of Kangfuxin solution on chemo/radiotherapy-induced mucositis in nasopharyngeal carcinoma patients: a multicenter, prospective randomized phase III clinical study, J. Evidence-Based Complementary Altern. Med. 2016 (2016) 8692343.
[8] J.S. Boateng, K.H. Matthews, H.N. Stevens, G.M. Eccleston, Wound healing dressings and drug delivery systems: a review, J. Pharmacol. Sci. 97 (2008) 2892–2923.
[9] J. Boateng, O. Catanzano, Advanced therapeutic dressings for effective wound healing—a review, J. Pharmacol. Sci. 104 (2015) 3653–3680.

[10] S.S. Wijetunge, J.C. Wen, C.-K. Yeh, Y.Y. Sun, Lectin-conjugated liposomes as biocompatible, bioadhesive drug carriers for the management of oral ulcerative lesions, ACS Appl. Bio Mater. 1 (2018) 1487–1495.
[11] B.V. Slaughter, S.S. Khurshid, O.Z. Fisher, A. Khademhosseini, N.A. Peppas, Hydrogels in regenerative medicine, Adv. Mater. 21 (2009) 3307–3329.
[12] Y.S. Zhang, A. Khademhosseini, Advances in engineering hydrogels, Science 356 (2017), eaaf3627.
[13] D. Chouhan, N. Dey, N. Bhardwaj, B.B. Mandal, Emerging and innovative approaches for wound healing and skin regeneration: current status and advances, Biomaterials 216 (2019) 119267.
[14] Y.-H. Tsou, J. Khoneisser, P.-C. Huang, X.Y. Xu, Hydrogel as a bioactive material to regulate stem cell fate, Bioact. Mater. 1 (2016) 39–55.
[15] W.G. Liu, M. Wang, W. Cheng, W. Niu, M. Chen, M. Luo, C.X. Xie, T.T. Leng, L. Zhang, B. Lei, Bioactive antiinflammatory antibacterial hemostatic citrate-based dressing with macrophage polarization regulation for accelerating wound healing and hair follicle neogenesis, Bioact. Mater. 6 (2021) 721–728.
[16] C. Ghobril, M.W. Grinstaff, The chemistry and engineering of polymeric hydrogel adhesives for wound closure: a tutorial, Chem. Soc. Rev. 44 (2015) 1820–1835.
[17] J.M. Zhang, Y.N. Zhu, J.Y. Song, T. Xu, J. Yang, Y. Du, L. Zhang, Rapid and long-term glycemic regulation with a balanced charged immune-evasive hydrogel in T1DM mice, Adv. Funct. Mater. 29 (2019) 1900140.
[18] Y.Z. Bu, L.C. Zhang, G.F. Sun, F.F. Sun, J.H. Liu, F. Yang, P.F. Tang, D.C. Wu, Tetra-PEG based hydrogel sealants for in vivo visceral hemostasis, Adv. Mater. 31 (2019) 1901580.
[19] S. Peers, A. Montembault, C. Ladavière, Chitosan hydrogels for sustained drug delivery, J. Contr. Release 326 (2020) 150–163.
[20] Y. Wu, T.Q. Chang, W.Q. Chen, X.Y. Wang, J.J. Li, Y.Q. Chen, Y. Yu, Z.Y. Shen, Q. Yu, Y.X. Zhang, Release of VEGF and BMP9 from injectable alginate based composite hydrogel for treatment of myocardial infarction, Bioact. Mater. 6 (2021) 520–528.
[21] J. Koehler, F.P. Brandl, A.M. Goepferich, Hydrogel wound dressings for bioactive treatment of acute and chronic wounds, Eur. Polym. J. 100 (2018) 1–11.
[22] S. Cascone, G. Lamberti, Hydrogel-based commercial products for biomedical applications: a review, Int. J. Pharm. 573 (2020) 118803.
[23] G.P. Chen, Y.R. Yu, X.W. Wu, G.F. Wang, J.N. Ren, Y.J. Zhao, Bioinspired multifunctional hybrid hydrogel promotes wound healing, Adv. Funct. Mater. 28 (2018) 1801386.
[24] L. Wang, X.H. Zhang, K. Yang, Y.V. Fu, T.S. Xu, S.L. Li, D.W. Zhang, L.N. Wang, C. S. Lee, A novel double-crosslinking-double-network design for injectable hydrogels with enhanced tissue adhesion and antibacterial capability for wound treatment, Adv. Funct. Mater. 30 (2020) 1904156.
[25] D. Simões, S.P. Miguel, M.P. Ribeiro, P. Coutinho, A.G. Mendonça, I.J. Correia, Recent advances on antimicrobial wound dressing: a review, Eur. J. Pharm. Biopharm. 127 (2018) 130–141.
[26] A. Gupta, M. Kowalczuk, W. Heaselgrave, S.T. Britland, C. Martin, I. Radecka, The production and application of hydrogels for wound management: a review, Eur. Polym. J. 111 (2019) 134–151.
[27] M. Edmonds, A. Foster, Hyalofill: a new product for chronic wound management, Diabet. Foot 3 (2000) 29–30.
[28] S.H. Aswathy, U. Narendrakumar, I. Manjubala, Commercial hydrogels for biomedical applications, Heliyon 6 (2020), e03719.
[29] L.Y. Shi, Y.N. Zhao, Q.F. Xie, C.X. Fan, J. Hilborn, J.W. Dai, D.A. Ossipov, Moldable hyaluronan hydrogel enabled by dynamic metal–bisphosphonate coordination chemistry for wound healing, Adv. Healthcare Mater. 7 (2018) 1700973.
[30] G.M. Sun, Pro-regenerative hydrogel restores scarless skin during cutaneous wound healing, Adv. Healthcare Mater. 6 (2017) 1700659.
[31] Y.L. Zhang, L. Tao, S.X. Li, Y. Wei, Synthesis of multiresponsive and dynamic chitosan-based hydrogels for controlled release of bioactive molecules, Biomacromolecules 12 (2011) 2894–2901.
[32] S.J. Jin, L. Ma, Q. Xu, L.C. Guo, L.P. Ren, Z.J. Shao, L.T. Liu, X.Y. Ma, L.M. Zhou, J. G. Wang, Protective effects of Kangfuxin liquid (Periplaneta Americana extract) on chronic atrophic gastritis in rats via anti-oxidative stress and inhibition of COX-2, Int. J. Clin. Exp. Med. 9 (2016) 18221–18226.
[33] P.P. Chen, Y.M. Shen, H.X. Shi, X.Y. Ma, B.B. Lin, T. Xiao, F.Z. Wu, J.J. Zhu, Z. M. Li, J. Xiao, X.K. Li, H.Y. Zhang, F.N. Geng, Gastroprotective effects of Kangfuxin-against ethanol-induced gastric ulcer via attenuating oxidative stress and ER stress in mice, Chem. Biol. Interact. 260 (2016) 75–83.
[34] A. Villa, S.T. Sonis, Pharmacotherapy for the management of cancer regimen-related oral mucositis, Expet Opin. Pharmacother. 17 (2016) 1801–1807.
[35] C. Pulito, A. Cristaudo, C.L. Porta, S. Zapperi, G. Blandino, A. Morrone, S. Strano, Oral mucositis: the hidden side of cancer therapy, J. Exp. Clin. Canc. Res. 39 (2020) 210.
[36] Y.S. Li, X. Wang, Y.N. Fu, Y. Wei, L.Y. Zhao, L. Tao, Self-adapting hydrogel to improve the therapeutic effect in wound-healing, ACS Appl. Mater. Interfaces 10 (2018) 26046–26055.
[37] J. Mishra, J. Swain, A.K. Mishra, Molecular level understanding of sodium dodecyl sulfate (SDS) induced sol-gel transition of Pluronic F127 using fisetin as a fluorescent molecular probe, J. Phys. Chem. B 122 (2018) 181–193.
[38] S. Hitomi, K. Ono, K. Miyano, Y. Ota, Y. Uezono, M. Matoba, S. Kuramitsu, K. Yamaguchi, K. Matsuo, Y. Seta, Novel methods of applying direct chemical and mechanical stimulation to the oral mucosa for traditional behavioral pain assays in conscious rats, J. Neurosci. Methods 239 (2015) 162–169.
[39] K. Yamaguchi, K. Ono, S. Hitomi, M. Ito, T. Nodai, T. Goto, N. Harano, S. Watanabe, H. Inoue, K. Miyano, Distinct TRPV1-and TRPA1-based mechanisms underlying enhancement of oral ulcerative mucositis-induced pain by 5-fluorouracil, Pain 157 (2016) 1004–1020.
[40] M.A. Skeff, G.A.C. Brito, M.G. de Oliveira, C.M. Braga, M.M. Cavalcante, V. Baldim, R.C. Holanda-Afonso, C.M. Silva-Boghossian, A.P. Colombo, R.A. Ribeiro, V. Moura-Neto, R.F.C. Leitão, S-nitrosoglutathione accelerates recovery from 5-fluorouracil-induced oral mucositis, PloS One 9 (2014), e113378.
[41] W.J. Zhang, W.G. Xu, C. Ning, M.Q. Li, G.Q. Zhao, W.Q. Jiang, J.X. Ding, X.S. Chen, Long-acting hydrogel/microsphere composite sequentially releases dexmedetomidine and bupivacaine for prolonged synergistic analgesia, Biomaterials 181 (2018) 378–391.
[42] B. Deng, L.Q. Jia, L. Pan, A.P. Song, Y.Y. Wang, H.Y. Tan, Q. Xiang, L.L. Yu, D. D. Ke, Wen-Luo-Tong prevents glial activation and nociceptive sensitization in a rat model of oxaliplatin-induced neuropathic pain, J. Evidence-Based Complementary Altern. Med. 2016 (2016) 3629489.
[43] W. Römisch-Margl, C. Prehn, R. Bogumil, C. Röhring, K. Suhre, J. Adamski, Procedure for tissue sample preparation and metabolite extraction for high-throughput targeted metabolomics, Metabolomics 8 (2012) 133–142.
[44] S.B. Ribeiro, A.A. de Araujo, R.F. de Araujo Junior, G.A. de Castro Brito, R. C. Leitao, M.M. Barbosa, V.B. Garcia, A.C. Medeiros, C.A.C.X. de Medeiros, Protective effect of dexamethasone on 5-FU-induced oral mucositis in hamsters, PloS One 12 (2017), e0186511.
[45] A.A. de Araújo, H. Varela, C.A.C.X. de Medeiros, G.A. de Castro Brito, K.C. de Lima, L.M. de Moura, R.F. de Araújo Júnior, Azilsartan reduced TNF-α and IL-1β levels, increased IL-10 levels and upregulated VEGF, FGF, KGF, and TGF-α in an oral mucositis model, PloS One 10 (2015), e0116799.
[46] X. Zhao, H. Wu, B.L. Guo, R.N. Dong, Y.S. Qiu, P.X. Ma, Antibacterial antioxidant electroactive injectable hydrogel as self-healing wound dressing with hemostasis and adhesiveness for cutaneous wound healing, Biomaterials 122 (2017) 34–47.
[47] M. Guvendiren, S. Yang, J.A. Burdick, Swelling-induced surface patterns in hydrogels with gradient crosslinking density, Adv. Funct. Mater. 19 (2009) 3038–3045.
[48] X.J. Lei, D.D. Ye, J. Chen, S. Tang, P.C. Sun, L.Y. Chen, A. Lu, Y.M. Du, L.N. Zhang, Customizable multi-dimensional self-wrinkling structure constructed via modulus gradient in chitosan hydrogels, Chem. Mater. 31 (2019) 10032–10039.
[49] F.F. Sun, Y.Z. Bu, Y.R. Chen, F. Yang, J.K. Yu, D.C. Wu, An injectable and instant self-healing medical adhesive for wound sealing, ACS Appl. Mater. Interfaces 12 (2020) 9132–9140.
[50] T. Su, M.Y. Zhang, Q.K. Zeng, W.H. Pan, Y.J. Huang, Y.N. Qian, W. Dong, X.L. Qi, J. L. Shen, Mussel-inspired agarose hydrogel scaffolds for skin tissue engineering, Bioact. Mater. 6 (2021) 579–588.
[51] N.B. Shelke, R. James, C.T. Laurencin, S.G. Kumbar, Polysaccharide biomaterials for drug delivery and regenerative engineering, Polym. Adv. Technol. 25 (2014) 448–460.
[52] J. Li, A.D. Celiz, J. Yang, Q. Yang, I. Wamala, W. Whyte, B.R. Seo, N.V. Vasilyev, J. J. Vlassak, Z. Suo, D.J. Mooney, Tough adhesives for diverse wet surfaces, Science 357 (2017) 378–381.
[53] S. Bayer, H.O. Kazancioglu, A.H. Acar, N. Demirtas, N.O. Kandas, Comparison of laser and ozone treatments on oral mucositis in an experimental model, Laser Med. Sci. 32 (2017) 673–677.
[54] J.C. Wheeler, J.A. Woods, M.J. Cox, R.W. Cantrell, F.H. Watkins, R.F. Edlich, Evolution of hydrogel polymers as contact lenses, surface coatings, dressings, and drug delivery systems, J. Long Term Eff. Med. Implants 6 (1996) 207–217.
[55] L.E. Reynolds, F.J. Conti, M. Lucas, R. Grose, S. Robinson, M. Stone, G. Saunders, C. Dickson, R.O. Hynes, A. Lacy-Hulbert, Accelerated re-epithelialization in β3-integrin-deficient-mice is associated with enhanced TGF-β1 signaling, Nat. Med. 11 (2005) 167–174.
[56] L. Nibali, S. Fedele, F. D'aiuto, N. Donos, Interleukin-6 in oral diseases: a review, Oral Dis. 18 (2012) 236–243.
[57] H.Y. Chen, J. Erndt-Marino, P. Diaz-Rodriguez, J. Kulwatno, A.C. JimenezVergara, S.L. Thibeault, M.S. Hahn, In vitro evaluation of anti-fibrotic effects of select cytokines for vocal fold scar treatment, J. Biomed. Mater. Res. B Appl. Biomater. 107 (2019) 1056–1067.
[58] P. Wang, S.B. Huang, Z.C. Hu, W. Yang, Y. Lan, J.Y. Zhu, A. Hancharou, R. Guo, B. Tang, In situ formed anti-inflammatory hydrogel loading plasmid DNA encoding VEGF for burn wound healing, Acta Biomater. 100 (2019) 191–201.
[59] Y. Zhao, Z.H. Li, S.L. Song, K.R. Yang, H. Liu, Z. Yang, J.C. Wang, B. Yang, Q. Lin, Skin-inspired antibacterial conductive hydrogels for epidermal sensors and diabetic foot wound dressings, Adv. Funct. Mater. 29 (2019) 1901474.
[60] F.G. Basso, D.G. Soares, T.N. Pansani, L.M. Cardoso, D.L. Scheffel, C.A. de Souza Costa, J. Hebling, Proliferation, migration, and expression of oral-mucosalhealing-related genes by oral fibroblasts receiving low-level laser therapy after inflammatory cytokines challenge, Laser Surg. Med. 48 (2016) 1006–1014.
[61] S. Werner, R. Grose, Regulation of wound healing by growth factors and cytokines, Physiol. Rev. 83 (2003) 835–870.
[62] M.A. Seeger, A.S. Paller, The roles of growth factors in keratinocyte migration, Adv. Wound Care 4 (2015) 213–224.
[63] J.K. Choi, J.-H. Jang, W.-H. Jang, J. Kim, I.-H. Bae, J. Bae, Y.-H. Park, B.J. Kim, K.-M. Lim, J.W. Park, The effect of epidermal growth factor (EGF) conjugated with low-molecular-weight protamine (LMWP) on wound healing of the skin, Biomaterials 33 (2012) 8579–8590.
[64] A.D. Kandhare, J. Alam, M.V.K. Patil, A. Sinha, S.L. Bodhankar, Wound healing potential of naringin ointment formulation via regulating the expression of inflammatory, apoptotic and growth mediators in experimental rats, Pharm. Biol. 54 (2016) 419–432.
[65] N. Subramaniam, J.J. Petrik, M.K. Vickaryous, VEGF, FGF-2 and TGFβ expression in the normal and regenerating epidermis of geckos: implications for epidermal homeostasis and wound healing in reptiles, J. Anat. 232 (2018) 768–782.

[66] S. Barrientos, O. Stojadinovic, M.S. Golinko, H. Brem, M. Tomic-Canic, Growth factors and cytokines in wound healing, Wound Repair Regen. 16 (2008) 585–601.
[67] N.-M. An, D.-D. Kim, Y.-H. Shin, C.-H. Lee, Development of a novel soft hydrogel for the transdermal delivery of testosterone, Drug Dev. Ind. Pharm. 29 (2003) 99–105.
[68] X.Y. Mao, R.Y. Cheng, H.B. Zhang, J.H. Bae, L.Y. Cheng, L. Zhang, L.F. Deng, W. G. Cui, Y.G. Zhan, H.A. Santos, X.M. Sun, Self-healing and injectable hydrogel for matching skin flap regeneration, Adv. Sci. 6 (2019) 1801555.
[69] Y.F. Ma, M. Lin, G.Y. Huang, Y.H. Li, S.Q. Wang, G.Q. Bai, T.J. Lu, F. Xu, 3D spatiotemporal mechanical microenvironment: a hydrogel-based platform for guiding stem cell fate, Adv. Mater. 30 (2018) 1705911.
[70] L.L. Zhao, L.J. Niu, H.Z. Liang, H. Tan, C.Z. Liu, F.Y. Zhu, pH and glucose dual-responsive injectable hydrogels with insulin and fibroblasts as bioactive dressings for diabetic wound healing, ACS Appl. Mater. Interfaces 9 (2017) 37563–37574.
[71] S.F. Khattak, S.R. Bhatia, S.C. Roberts, Pluronic F127 as a cell encapsulation material: utilization of membrane-stabilizing agents, Tissue Eng. 11 (2005) 974–983.
[72] H.H. Jung, K. Park, D.K. Han, Preparation of TGF-β1-conjugated biodegradable pluronic F127 hydrogel and its application with adipose-derived stem cells, J. Contr. Release 147 (2010) 84–91.
[73] H. Lee, B.G. Choi, H.J. Moon, J. Choi, K. Park, B. Jeong, D.K. Han, Chondrocyte 3D-culture in RGD-modified crosslinked hydrogel with temperature-controllable modulus, Macromol. Res. 20 (2012) 106–111.
[74] E. Lippens, I. Swennen, J. Gironès, H. Declercq, G. Vertenten, L. Vlaminck, F. Gasthuys, E. Schacht, R. Cornelissen, Cell survival and proliferation after 33 encapsulation in a chemically modified Pluronic® F127 hydrogel, J. Biomater. Appl. 27 (2013) 828–839.